Mechanics of Advanced Composite Structures

Journal homepage: https://macs.semnan.ac.ir/

Semnan University

ISSN: 2423-7043

Research Article

Effect of Aspect Ratio on the Workability of AA6082/Metakaolin/Nano Silicon Nitride Composites: An Experimental Investigation and Predictive Modeling using RSM and ANN

Renjin Jasmine Bright[a] , Raja Varadharaj[a], Selvakumar Gurusamy[b], Hariharasakthisudhan Ponnarengan[c], Vikas Khalkar[d]

[a]*Department of Production Engineering, PSG College of Technology, Coimbatore, 641004, Tamil Nadu, India*
[b]*Department of Rural & Entrepreneurship Development, National Institute of Technical Teachers Training and Research, NITTTR, Chennai-600113, Tamil Nadu India.*
[c]*Department of Mechanical Engineering, Dr. Mahalingam College of Engineering and Technology, Pollachi 642003, Tamil Nadu, India*
[d]*Department of Mechanical Engineering, Gharda Institute of Technology, Khed, Ratnagiri, 415708, Maharashtra, India*

ARTICLE INFO

Article history:

Received:
Revised:
Accepted:

Keywords:

Composites;
Workability;
Compression;
Microstructure;
RSM;
ANN.

ABSTRACT

Understanding the impact of aspect ratio on the deformation and load-bearing capacity of aluminium matrix composites is crucial in tailoring their forming performance. In this study, aluminium alloy (AA) 6082/Metakaolin (MK)/nano silicon nitride (Si_3N_4) composites containing 7.5 wt.% MK and 1.5 wt.% Si_3N_4 were fabricated using ultrasonic cavitation-assisted stir casting and tested under quasi-static compression with cylindrical specimens of aspect ratios 0.5, 1, and 1.5 in both as-cast and T6 heat-treated conditions. The results showed that lower aspect ratios significantly enhanced workability. The as-cast composite at aspect ratio 0.5 sustained compressive deformation up to a 50% reduction in height without visible cracks, achieving a maximum axial stress of 573.25 MPa. The T6 heat-treated samples exhibited a maximum compressive strength of 543.31 MPa and fractured at lower strain due to embrittlement caused by eutectic Si and Mg_2Si phases. Microstructural analysis indicated pore closure as the governing deformation mechanism in as-cast specimens, while brittle fracture dominated the T6 samples. Instantaneous strain hardening exponent (n_i) and strength coefficient (k_i) trends confirmed contributions from both matrix and geometric work hardening during deformation. In order to predict the workability parameters for different aspect ratios and loadings, response surface methodology (RSM) and artificial neural network (ANN) were employed. ANN yielded superior prediction accuracy for the workability parameters compared to RSM. These findings confirm that aspect ratio strongly controls the deformation mechanisms, with shorter cylindrical specimens offering optimum workability for practical forming operations.

1. Introduction

The effect of numerous particulate reinforcements on the mechanical and wear properties of aluminium matrix composites has been investigated by several researchers for the past two decades [1-9]. Selvam et al. [3] developed AA6061 matrix – fly ash composites with minimal porosity using the compocasting technique. The presence of fly ash improved the strength and hardness of the composites as a result of grain refinement. AA6061 composites reinforced with nano Si_3N_4 and Al_2O_3 particles showed good compressive strength, toughness, and hardness at the expense of ductility [4]. AA6082-MK composites developed through stir casting showed improved strength and wear

*** Corresponding author.**
E-mail address: renjin1990@gmail.com

Cite this article as:
Renjin J Bright, Raja V, Selvakumar G, Hariharasakthisudhan P and V Khalkar 2025. Effect of Aspect Ratio on the Workability of AA6082/Metakaolin/Nano Silicon Nitride Composites: An Experimental Investigation and Predictive Modeling using RSM and ANN. *Mechanics of Advanced Composite Structures*, 12(1), pp. xx-xx
https://doi.org/10.22075/MACS.2024.39315.2050

resistance, but reduced ductility [5]. Hillary et al. [6] reported on the reduction in porosity and improvement in mechanical properties of AA6061 composites while reinforced with coconut shell ash and silicon carbide particles. Kumar et al. [7] synthesized AA6082 composites reinforced with zirconium oxide and coconut shell ash using the powder metallurgy route. The composites possessed good mechanical properties as a result of the fine and uniform distribution of reinforcements. Gupta et al. [8] developed AA7075 composites reinforced with varying proportions of rice husk ash and carbonized eggshells using stir-casting. The results indicated that the addition of the agro-waste fillers decreased density and increased porosity of the composites. Kamatchi et al. [9] developed Al matrix composites using bone ash as reinforcement via the powder metallurgy route. The composites possessed high compressive strength but low ductility.

Reinforcing a ductile aluminium matrix with ceramic particulates generally reduces the ductility and workability of the resulting composite material. Processing methods such as stir casting might result in the formation of particle clusters and voids in composites. Hence, it is necessary to assess the workability behaviour of ceramic particulate-reinforced aluminium matrix composites processed via stir casting. Moreover, knowledge regarding the workability of composites is essential for predicting the final shape before failure of real-time structural components developed using the same composite material, designing an effective forming process, and designing dies for the forming process. In most forming processes, such as rolling, forging, swaging, etc., the state of stress is compressive. The cold upsetting of cylindrical samples is one of the most significant tests used to determine the formability and plastic deformation behaviour of materials under compressive loading [10-22].

The type and the particle size of the reinforcements govern the tensile strength, ductility, and workability of the composite material. Bright *et al.* [10] investigated the effect of reinforcing hybrid MK and Si_3N_4 nanoparticles in the AA6082 matrix through ultrasonic cavitation-assisted stir-casting. The mechanical properties and workability of the composites were studied by the authors for different weight fractions of the reinforcements. The workability of the composites was studied by maintaining a constant aspect ratio of 1.5. The composite sample with 7.5 weight fraction (wt.%) MK and 1.5 wt.% Si_3N_4 was observed to possess good tensile strength, ductility, and workability. Narayanasamy *et al.* [15] investigated the workability of composites prepared using aluminium powder with a particle size of 100 µm as the matrix material, and SiC particles with three different particle sizes of 50 µm, 65 µm, and 120 µm as the reinforcement material. SiC particles were added to the aluminium matrix in the amounts of 5 wt.%, 10 wt.%, 15 wt.%, and 20 wt.%. The aspect ratio of the specimens utilized was 1.5. The formability index (β), strain hardening exponent (n), and strength coefficient (k) were evaluated to characterize the workability behaviour. Taha *et al.* [23] investigated the workability of aluminium matrix composites reinforced with SiC particles with particle sizes of 102 µm, 128 µm, and 158 µm. The composites were prepared by means of stir casting, squeeze casting, and powder metallurgy and were subjected to heat treatment. The cold upsetting test was conducted on composite samples with a diameter of 8 mm and height of 8 mm. Composites prepared using the stir casting technique exhibited better workability behaviour than those processed via powder metallurgy and squeeze casting. Thangadurai *et al.* [24] investigated the workability behaviour of AA6061–micro B_4C (45 µm) particle-reinforced metal matrix composites. The diameter of the specimen was 20 mm, and the aspect ratio was maintained as one. The axial stress, hoop stress, and hydrostatic stress increased with increasing reinforcement weight fraction. Sakthi Sadhasivam *et al.* [25] reported that the formability index of AA6061/micro ZnO particle composites improved with increasing weight fraction of ZnO particles. Sivasankaran *et al.* [26] explored the possibility of predicting the workability parameters of Al/SiC composites using ANN models. Factors such as the SiC particle size, SiC weight fraction, relative density, and load were used as the input parameters to predict the workability parameters such as the axial stress, hoop stress, axial strain, hoop strain, strain hardening exponent, and strength coefficient. Hassani et al. [27] analyzed the effect of porosity and reinforcement on the cold upsetting of Al-silicon carbide composites produced via powder metallurgy and mechanical alloying. Smaller SiC particles and higher reinforcement volume reduced porosity, increased work hardening, and improved forming characteristics.

The aspect ratio of the cylindrical composite samples is a significant factor in determining the mode of deformation of the composites under quasistatic compression. A higher aspect ratio leads to buckling with nonuniform stress distribution and localized strain hardening. The aspect ratio of the samples also affects the friction between the samples and the die, which further indicates the necessity of using suitable lubricants [20, 28]. Narayanasamy *et al.* [19] investigated the workability behaviour of Al-Al_2O_3 composites developed using the powder

metallurgy technique. Cylindrical specimens with a diameter of 27.80 mm and aspect ratios of 0.35, 0.56, and 0.72 were selected for the study. The forming limit diagrams were plotted between the axial strain and different stresses, such as the hoop stress, axial stress, and hydrostatic stress (mean stress). The authors reported that the formability index decreased with decreasing aspect ratio. Sivaraj *et al.* [29] determined the effect of the TiC reinforcement particle size and aspect ratio (0.75 and 1) of the cylindrical samples on the workability behaviour of the Al-TiC composites processed through the powder metallurgy route. It has been inferred that the composites with TiC of particle size less than 200 nm and aspect ratio 0.75 possessed better work-hardening. Hariharasakthisudhan *et al.* [12] determined the workability behaviour of AA6061 matrix composites reinforced with exhausted alkaline battery powder via stir casting. The composite samples for the workability study were prepared with aspect ratios of 0.5, 1, and 1.5, and the sample with an aspect ratio of 0.5 was reported to withstand the maximum compressive load before failure.

The workability and deformation behavior of aluminium matrix composites are strongly influenced by reinforcement type, processing route, and specimen geometry, particularly aspect ratio, which governs load distribution, strain localization, and the onset of failure during forming operations. From the extensive literature review, it has been noted that most of the researchers focused on the study of the workability behaviour of aluminium matrix composites synthesized via powder metallurgy [15-22]. Only a few researchers examined the same developed via stir casting. Limited research has focused on composites synthesized via ultrasonic cavitation-assisted stir casting, which offers improved particle distribution but may introduce porosity and clustering [12, 13, 23]. The necessity to study the influence of different aspect ratios of composite samples on the failure mode and load-carrying capacity of the composites has also been discussed by a few researchers.

This study aims to evaluate the influence of aspect ratio on the workability of AA6082 composites reinforced with metakaolin (MK) and nano silicon nitride (Si_3N_4) and to establish reliable predictive models for their deformation behavior. The novelty of this work lies in correlating experimental quasi-static compression results with microstructural mechanisms and in applying both response surface methodology (RSM) and artificial neural networks (ANN) to model and predict workability parameters across varying aspect ratios and loading conditions. The specific objectives are: (i) to fabricate AA6082/MK/Si_3N_4 composites using ultrasonic cavitation-assisted stir casting and subject them to quasi-static compression in both as-cast and T6 conditions; (ii) to analyze the role of aspect ratio on stress–strain response, strain hardening behavior, and deformation mechanisms; (iii) to perform microstructural characterization to identify dominant failure modes using SEM; and (iv) to develop and compare RSM and ANN predictive models for estimating key workability parameters. The composition of the reinforcement was judiciously selected based on the previous study [13]. The cylindrical composite samples for cold upsetting were prepared with three different aspect ratios of 0.5, 1, and 1.5, with the diameter held constant at 20 mm. The stress components, namely axial stress (σ_z), hoop stress (σ_θ), mean or hydrostatic stress (σ_m), and effective stress (σ_{eff}), were evaluated employing the mathematical relations explained in Narayanasamy *et al.* [17]. The instantaneous strain hardening exponent (n_i) and the instantaneous strength coefficient (k_i) were evaluated for each composite sample under every load step, and the values were plotted against the axial strain values to identify the nature of work hardening.

2. Materials and Methodology

The aluminium alloy AA6082, which possesses excellent cold workability, was utilized as the matrix material. MK particles (average particle size 200 nm) premixed with Si_3N_4 particles (average particle size 50 nm) were used as the reinforcement phase. The weight fraction of the reinforcements was fixed as 7.5 wt.% for the MK particles and 1.5 wt.% for Si_3N_4 particles based on the previous study conducted by the authors [13]. The density of AA6082 is 2.69 g/cm^3, and that of MK particles is 2.6 g/cm^3. The 99% pure nano-Si_3N_4 powder with a density of 3.17 g/cm^3 was premixed before being directly supplied into the AA6082 melt during the stir casting process to avoid agglomeration [5,13]. Figure 1 shows the SEM and EDAX images of the premixed reinforcement particles.

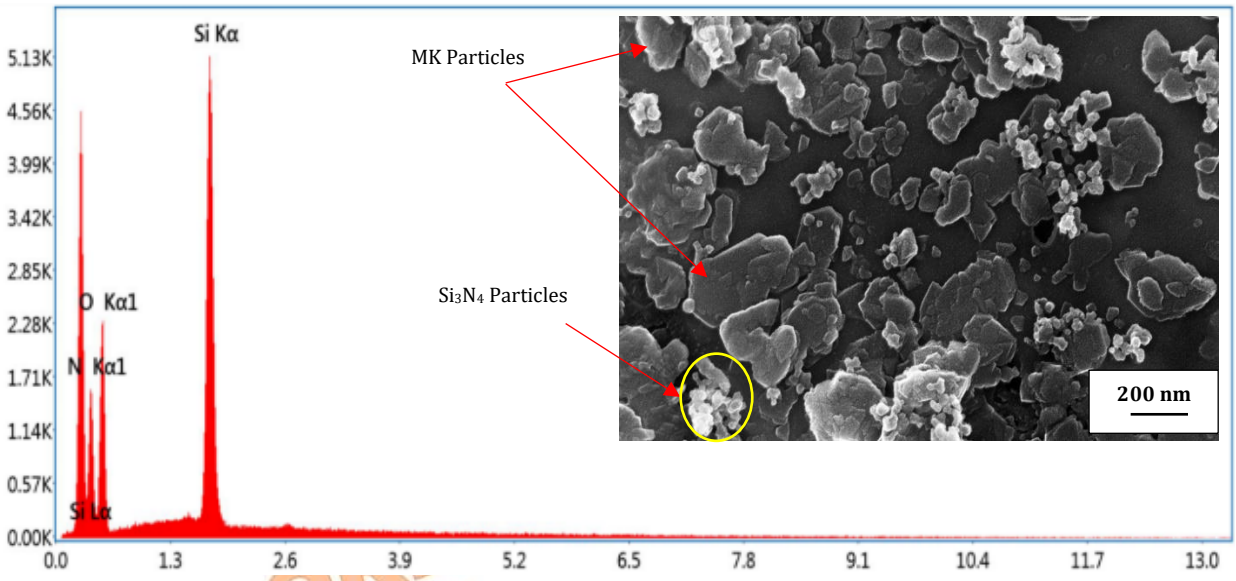

Fig. 1. SEM and EDAX images of the mixed reinforcement particles (7.5 wt.% MK + 1.5 wt.% Si_3N_4)

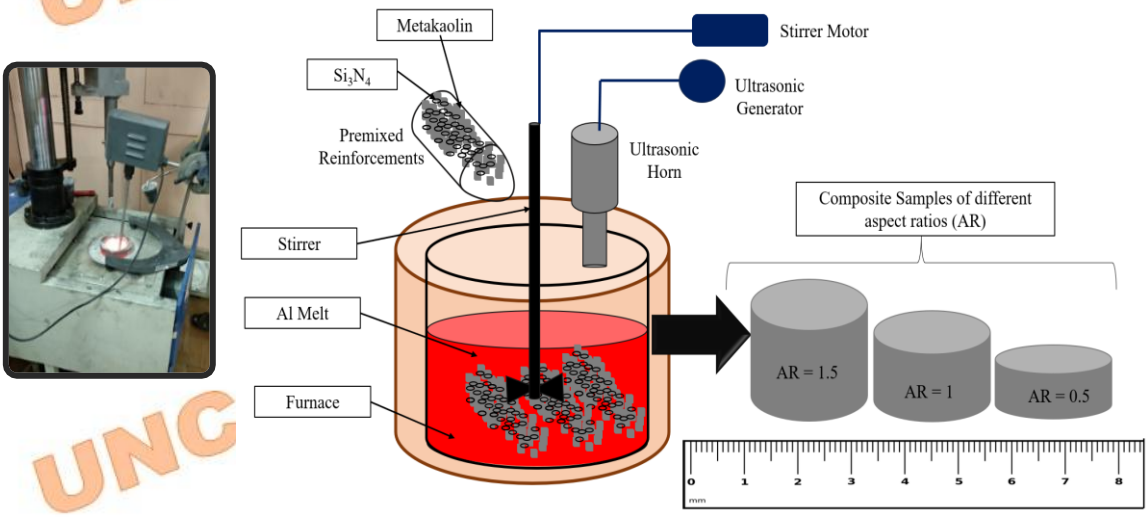

Fig. 2. Schematic representation of the synthesis of composites

The composites were synthesized through the ultrasonic cavitation-assisted stir-casting process as described by Bright *et al.* [5]. Figure 2 shows a schematic representation of the ultrasonication-assisted stir casting technique used for processing the composites. The ultrasonication setup consisted of a stepped titanium horn and transducer assembly, an ultrasonic generator with a power rating of 2 kW, and a 20 kHz output frequency inert gas supply. The AA6082 rods were melted in the furnace by maintaining a temperature of 750 °C, and the premixed MK and Si_3N_4 were preheated at 400 °C for 2 hours and supplied to the melt. Then, the melt was stirred for 10 minutes at 700 rpm initially and subjected to ultrasonic vibration at 20 kHz frequency for 20 minutes, followed by pouring into specially prepared dies. The composites were then subjected to T6 heat treatment. The T6 heat treatment process involves solutionizing the composite sample at 530 °C for 1 hr, followed by water quenching and artificial ageing for 8 hours at 175 °C [5]. The as-cast and T6 composites were machined to cylindrical forms with a diameter of 20 mm and aspect ratios of 0.5, 1, and 1.5, as shown in Fig. 3, and subjected to the quasistatic compression tests. Figures 4 and 5 show the SEM, EDAX, and elemental mapping images of the cross-sections of the as-cast and T6 composite samples, respectively.

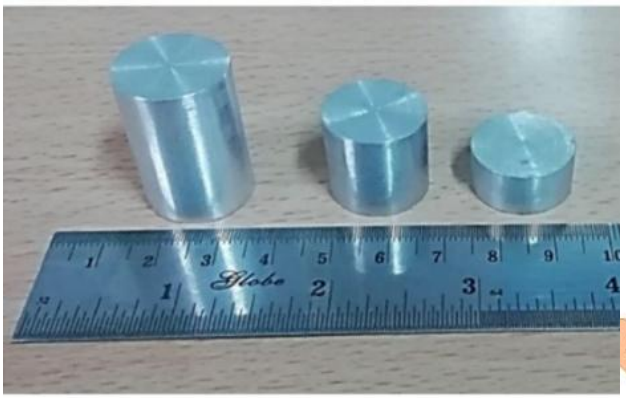

Fig. 3. Composite samples with different aspect ratios (1.5, 1, and 0.5) for the workability study

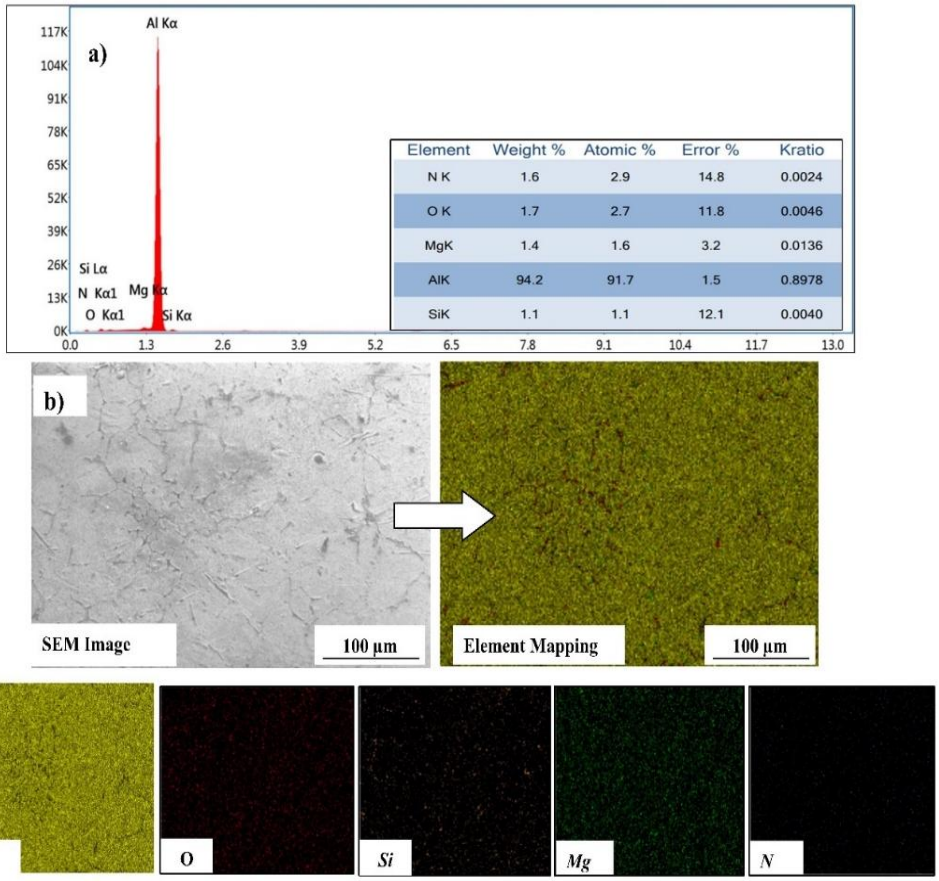

Fig. 4. a) EDAX, b) SEM and elemental mapping images of the cross-section of the as-cast composite sample [13]

The cylindrical composite samples were cold upset between two steel dies tempered and hardened to RC 46-50 [20]. The contact surface of the dies was mirror polished, and during the cold upsetting test, the die set was well lubricated with graphite particles with an average particle size of 50 µm to reduce the barreling effect caused by friction [17, 20]. The specimens were loaded in steps of 20 kN until a visible crack was generated or the height was reduced to 50%, whichever was the first. The stress values indicate the load-bearing capacity of the composite samples, while the strain-hardening behaviour could be explained by the strain-hardening exponent and strength coefficient. The strain hardening exponent values lie between 0 and 1 for most of the materials. A material is considered to be a perfectly plastic solid when the value of n is 1, and when the value of n is 0, the material is 100 % elastic solid. The value of n for most of the metals lies between 0.10 and 0.50. The strength coefficient value constitutes the extrapolated value of the true stress at a true strain of 1. During quasistatic loading, the instantaneous values of the strain hardening exponent and strength coefficient could be used to identify the work hardening behaviour of the composites under various stages of loading.

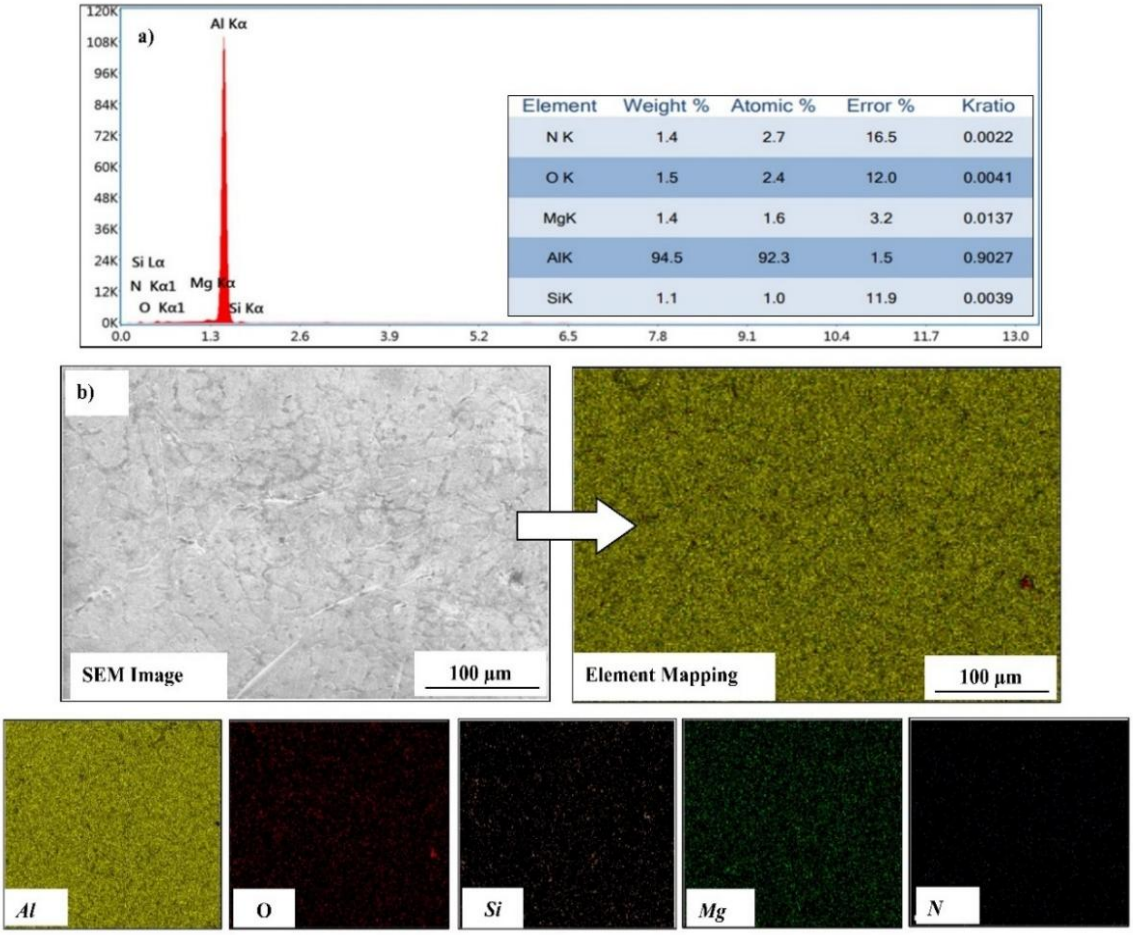

Fig. 5. a) EDAX, b) SEM, and elemental mapping images of the cross-section of the T6 heat-treated composite sample

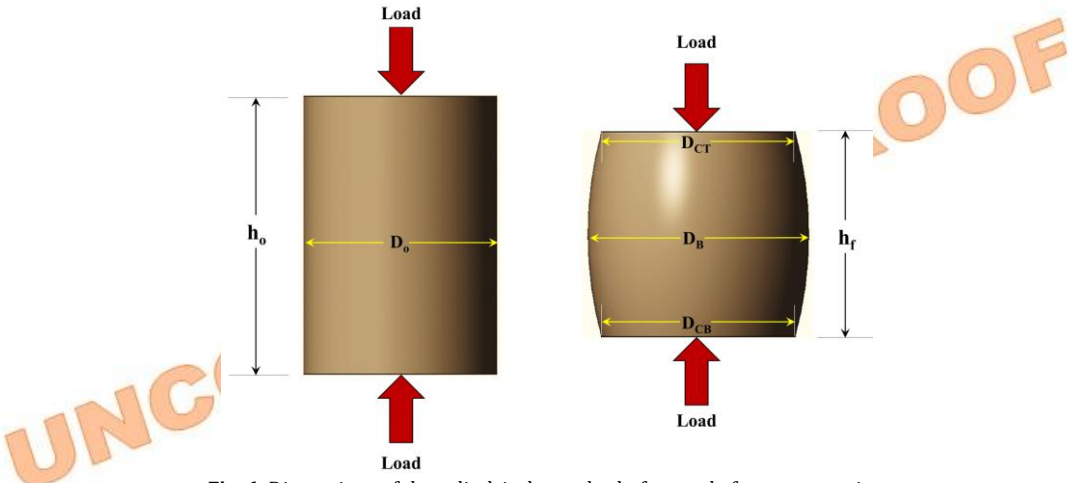

Fig. 6. Dimensions of the cylindrical samples before and after compression

The parameters involved in predicting the workability behaviour of cylindrical samples subjected to quasistatic compression are the true axial stress (σ_z), true hoop stress (σ_θ), hydrostatic stress (σ_m), axial strain (ε_z), hoop strain (ε_θ), and instantaneous strain-hardening parameters such as

*** Corresponding author.**
E-mail address: renjin1990@gmail.com

Cite this article as:
Renjin J Bright, Raja V, Selvakumar G, Hariharasakthisudhan P and V Khalkar 2025. Effect of Aspect Ratio on the Workability of AA6082/Metakaolin/Nano Silicon Nitride Composites: An Experimental Investigation and Predictive Modeling using RSM and ANN. *Mechanics of Advanced Composite Structures*, 12(1), pp. xx-xx
https://doi.org/10.22075/MACS.2024.39315.2050

the instantaneous strain hardening exponent (n_i) and instantaneous strength coefficient (k_i). The empirical relations to evaluate these workability parameters are illustrated in Equations 1 to 9 [15, 17].

True axial stress

$$\sigma_z = \frac{\text{Load (P)}}{\text{Contact Surface Area } (A_c)} \quad (1)$$

True Axia Strain

$$\varepsilon_z = ln\left(\frac{h_0}{h_f}\right) \quad (2)$$

where h_0 and h_f represent the heights of the composite samples before and after deformation, respectively, as shown in Fig. 6.

Hoop stress

$$\sigma_\theta = \left(\frac{1+2\alpha}{2+\alpha}\right)\sigma_z \quad (3)$$

where 'α' represents Poisson's ratio given by the equation,

$$\alpha = \frac{\varepsilon_\theta}{2\varepsilon_z} \quad (4)$$

Hoop strain

$$\varepsilon_\theta = ln\left(\frac{D_C}{D_0}\right) \quad (5)$$

where D_0 is the initial diameter of the composite sample, and D_C is the average value of contact diameters on the top (D_{CT}) and bottom (D_{CB}) of the composite sample after deformation, as shown in Fig. 6. D_B represents the bulge diameter.

Hydrostatic stress

$$\sigma_m = \frac{1}{3}(\sigma_z \pm \sigma_\theta) \quad (6)$$

Effective stress

$$\sigma_{eff} = (0.5 + \alpha)\,[3(1 + \alpha + \alpha^2)]^{0.5}\,\sigma_z \quad (7)$$

Instantaneous strain hardening exponent (n_i)

$$n_i = \frac{ln\left(\frac{\sigma_m}{\sigma_{m-1}}\right)}{ln\left(\frac{\varepsilon_m}{\varepsilon_{m-1}}\right)} \quad (8)$$

Instantaneous strength coefficient (k_i)

$$k_i = \frac{(\sigma_m - \sigma_{m-1})}{(\varepsilon_m^n - \varepsilon_{m-1}^n)} \quad (9)$$

3. RESULTS AND DISCUSSION

3.1 Variation in the workability parameters with axial strain

The variation in the stress components (σ_z, σ_θ, σ_m, and σ_{eff}) with axial strain for the as-cast and T6 composite samples of aspect ratios 0.5, 1, and 1.5 is shown in Fig. 7 (a-c) and Fig. 8 (a-c), respectively.

In order to plot the stress-strain curves, the sense of σ_z was taken as negative, as the loading is compressive. The σ_θ is positive since the cylindrical samples bulge, as shown in Fig. 6. The computed values of σ_m and σ_{eff} indicate that the hydrostatic stress is compressive and the effective stress is tensile. The σ_θ values were less than the σ_z values since the graphite lubricant reduces friction between the contact surfaces of the dies and sample, which in turn limits the radial expansion of the samples by reducing the buckling and barreling effects. The failure strain values indicate that the as-cast composites are subjected to extensive deformation before fracture compared to the T6 samples. From Fig. 7 and Fig. 8, it can be observed that compressive stresses increased as the aspect ratio decreased. The as-cast composites with aspect ratios of 0.5 and 1 were able to sustain compressive deformation up to a 50% reduction in height without visible cracking. Specifically, the as-cast samples with aspect ratios of 0.5 and 1 reached maximum axial stresses of 573.27 MPa (strain 0.733) and 567.24 MPa (strain 0.719), respectively. In contrast, the sample with an aspect ratio of 1.5 failed prematurely, fracturing at a lower stress and strain of 476.32 MPa and 0.664. For the T6-treated composites, all specimens fractured before attaining 50% height reduction, reflecting their higher brittleness. Among them, the T6 sample with an aspect ratio of 0.5 exhibited the highest axial stress and strain of 543 MPa and 0.583, whereas the T6 sample with an aspect ratio of 1.5 recorded the lowest values, with a maximum stress of 397.28 MPa and strain of 0.577.

The microstructural study of the lateral surface (Fig. 7 and Fig. 8) of the composite samples revealed the possibility of pore closure as the major phenomenon responsible for the good workability of the composites. Similar observations were reported in a few other works [12, 13, 30]. The MK and nano Si_3N_4 reinforcement particles were bonded well to the matrix, which increased the load-bearing capacity of the composites by extending the deformation and delaying the fracture [13]. The well-bonded particles extended the failure by the dispersion strengthening mechanism, while the spots of the particle clusters might have acted as the sites for crack nucleation.

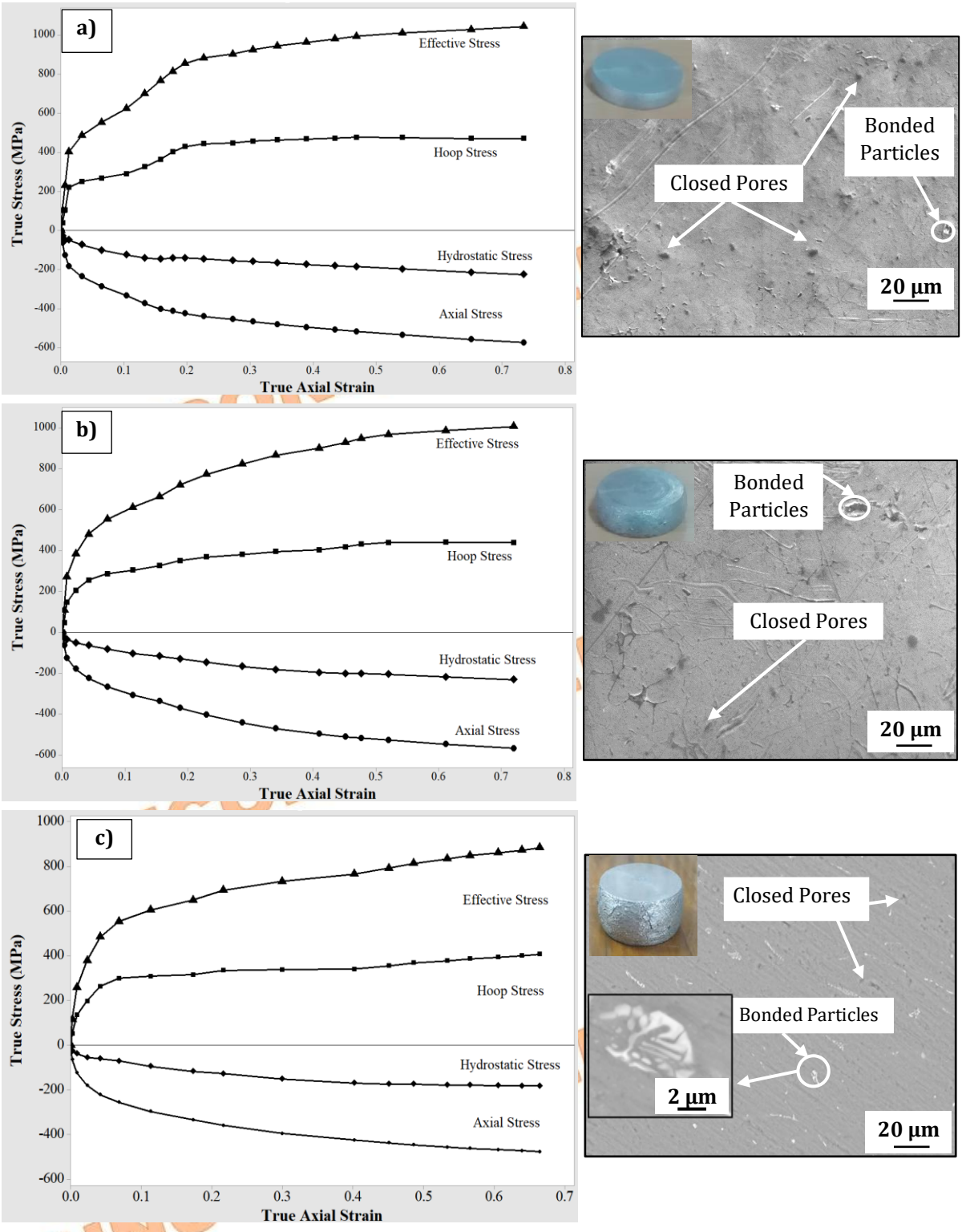

Fig. 7. Stress components and microstructure of the as-cast samples (a) aspect ratio = 0.5, (b) aspect ratio = 1, and (c) aspect ratio = 1.5 [13]

*** Corresponding author.**
E-mail address: *renjin1990@gmail.com*

Cite this article as:
Renjin J Bright, Raja V, Selvakumar G, Hariharasakthisudhan P and V Khalkar 2025. Effect of Aspect Ratio on the Workability of AA6082/Metakaolin/Nano Silicon Nitride Composites: An Experimental Investigation and Predictive Modeling using RSM and ANN. *Mechanics of Advanced Composite Structures*, 12(1), pp. xx-xx
https://doi.org/10.22075/MACS.2024.39315.2050

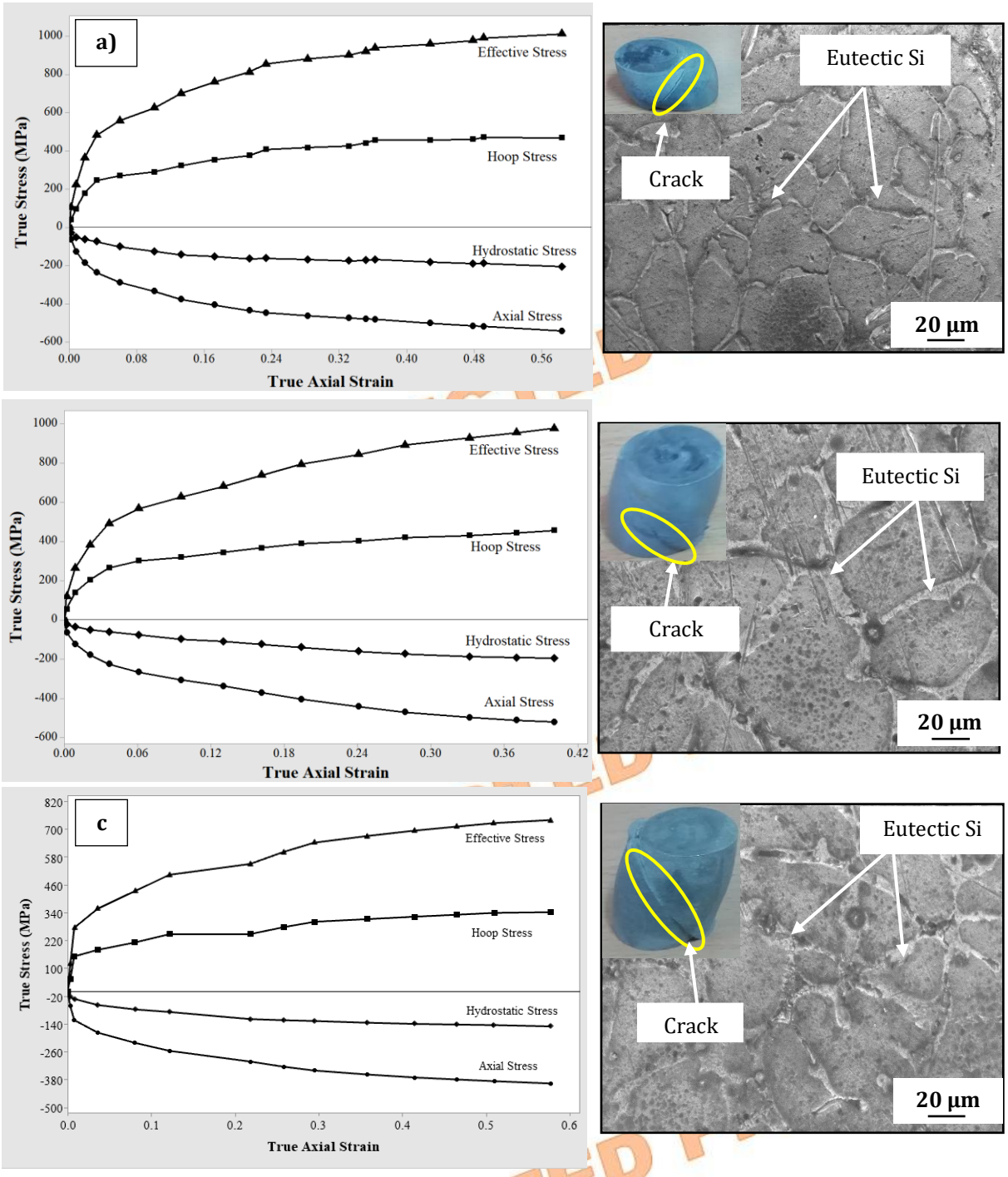

Fig. 8. Stress components and microstructure of the T6 samples (a) aspect ratio = 0.5, (b) aspect ratio = 1, (c) aspect ratio = 1.5

The porosity of the composite samples before and after cold-upsetting was estimated by means of the water immersion displacement method according to ASTM C135-2003 standards. The weight of the composite samples was initially measured in air and then in water using a physical weighing balance to calculate the experimental density. The theoretical density was estimated using the rule of mixture principle. The porosity (%) values evaluated using Equation 10 are depicted in Fig. 9.

$$\text{Poroty} = \frac{\rho_{\text{theoretical}} - \rho_{\text{experimental}}}{\rho_{\text{theoretical}}} \quad (10)$$

The theoretical and experimental densities were calculated using Equations 11 and 12.

$$\rho_{\text{theoretical}} = \rho_m \nu_m + \rho_r \nu_r \quad (11)$$

where ρ_m and ρ_r represent the density of the matrix and reinforcements; ν_m and ν_r represent the weight fraction of the matrix and reinforcements.

$$\rho_{\text{experimental}} = \frac{\text{mass in air}}{\text{mass in air} - \text{mass in water}} \quad (12)$$

From Fig.9, it could be noted that the composites after cold-upsetting showed a reduction in porosity, which quantifies the presence of closed pores observed in the microstructure. The T6 heat treatment process imparts greater resistance to compressive loading on the composite samples by means of grain refinement and precipitation hardening. The Si-rich eutectic formed during solidification acts as nucleation sites for new aluminium grains and contributes to grain refinement (Fig. 8 a-c). However, a higher amount of Si-eutectic induces brittleness. Moreover, during heat treatment, the Mg in AA6082 may react with Si to form brittle intermetallic Mg_2Si, which imparts strength to the composites by precipitation hardening. The reason for the fracture of T6 samples at lower values of axial strain may be due to the higher brittleness induced as a result of the formation of eutectic Si along the grain boundaries, as well as the possibility of fragmentation of eutectic Si [28]. Figure 10 shows the schematic representation of the modes of deformation in the composites under compression. The trends of ni and ki values were similar to those observed for the as-cast samples.

The n_i values under quasistatic compressive loading for the as-cast and T6 composite samples are shown in Fig. 11 (a and b), respectively. The ni values quantify the inherent ability of a material to resist deformation of the composites under axial loading. The k_i values of the as-cast and T6 composite samples shown in Fig. 12 (a and b), respectively, could be used to predict the compressive strength of the composites at different phases of deformation.

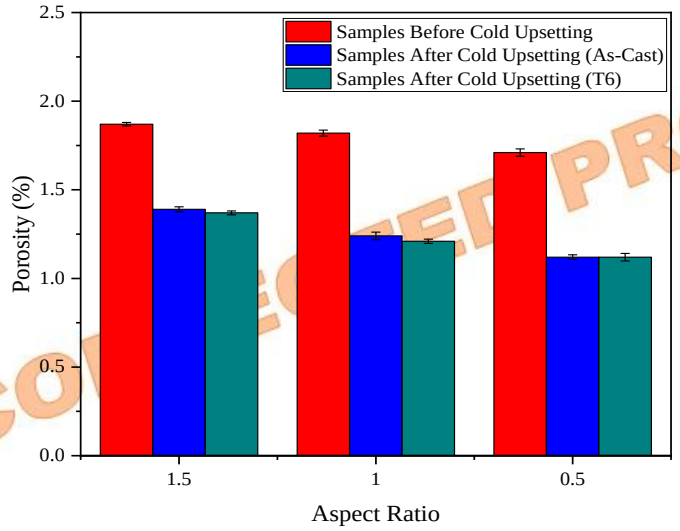

Fig. 9. Porosity of composite samples before and after cold upsetting

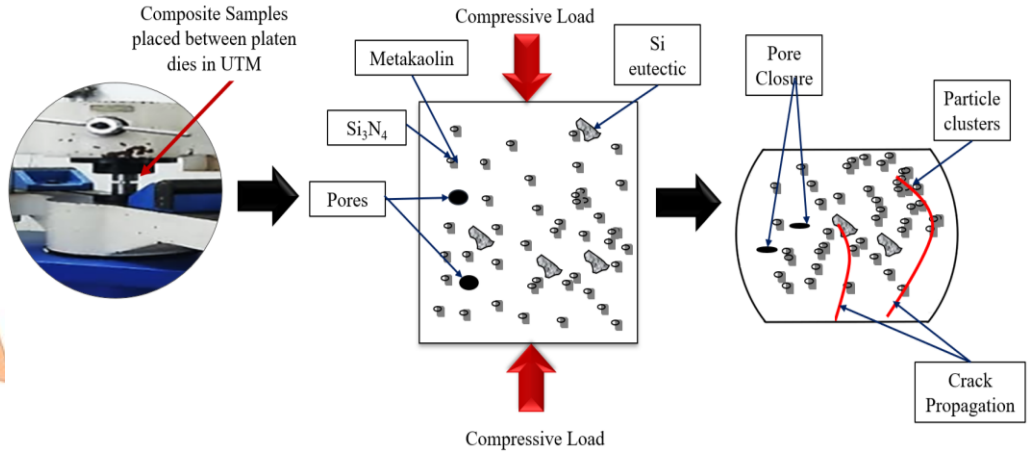

Fig. 10. Schematic representation of the modes of deformation in the AA6082/MK/nano Si_3N_4 composites under compression

*** Corresponding author.**
E-mail address: *renjin1990@gmail.com*

Cite this article as:
Renjin J Bright, Raja V, Selvakumar G, Hariharasakthisudhan P and V Khalkar 2025. Effect of Aspect Ratio on the Workability of AA6082/Metakaolin/Nano Silicon Nitride Composites: An Experimental Investigation and Predictive Modeling using RSM and ANN. *Mechanics of Advanced Composite Structures*, 12(1), pp. xx-xx
https://doi.org/10.22075/MACS.2024.39315.2050

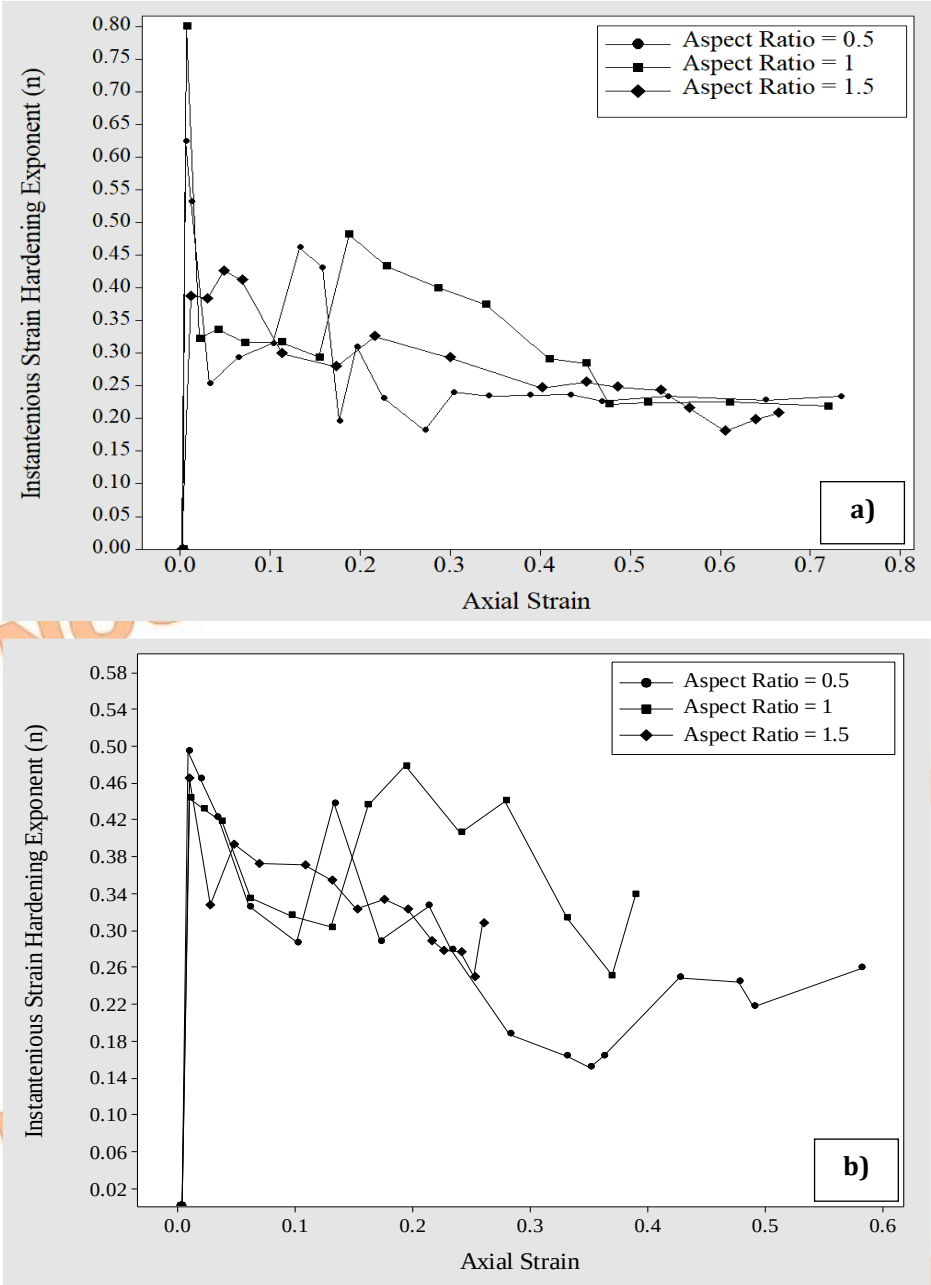

Fig. 11. Instantaneous strain hardening exponent of composite samples (a) as-cast (b) T6

From the stress-strain curves of both the as-cast and T6 composites (Fig. 7 and Fig.8), it can be observed that all the stress components increased rapidly with a slight increase in axial strain values during the initial phase of loading, followed by a gradual increase under further loading. From Fig. 11 and Fig. 12, it could be noted that the n_i and the k_i also reached their peak values at the initial phase of loading and decreased upon further loading. The initial increase in the stress components, as well as the n_i and the k_i values, could be attributed to the higher resistance to deformation offered by the aluminium matrix, and this phenomenon is referred to as matrix work hardening [16, 30]. After the initial barrier offered by the matrix, the stress components attained a slower rate of increase, and the n_i and the k_i values were reduced with an increase in axial strain due to the phenomenon termed geometric work hardening [18, 27]. However, the intermediate spikes observed in the n_i and the k_i values of the composite samples may be due to the resistance to the compressive loading offered by the particulate reinforcements.

During fracture, the n_i and the k_i values slightly increased, which is attributed to the dominance of matrix work hardening before the generation of cracks. The micrograph of the lateral surface of the composite as-cast samples (Fig. 7) with an aspect ratio of 1 and 0.5 shows some sites of pore closure as well as well-bonded particles that obstruct plastic deformation. This, in turn, could be attributed to the intermediate spikes observed in the strain hardening exponent-axial strain plots. Spots of pore closure and well-bonded particles can also be observed on the composite sample with an aspect ratio of

1.5, which is responsible for the spikes observed in the strain hardening exponent-axial strain plot [13]. The barrier to compressive loading induced by the reinforcement particles along with the Si-eutectic and Mg_2Si intermetallic phases may be attributed to the nature of the n_i and k_i plots of the T6 composites.

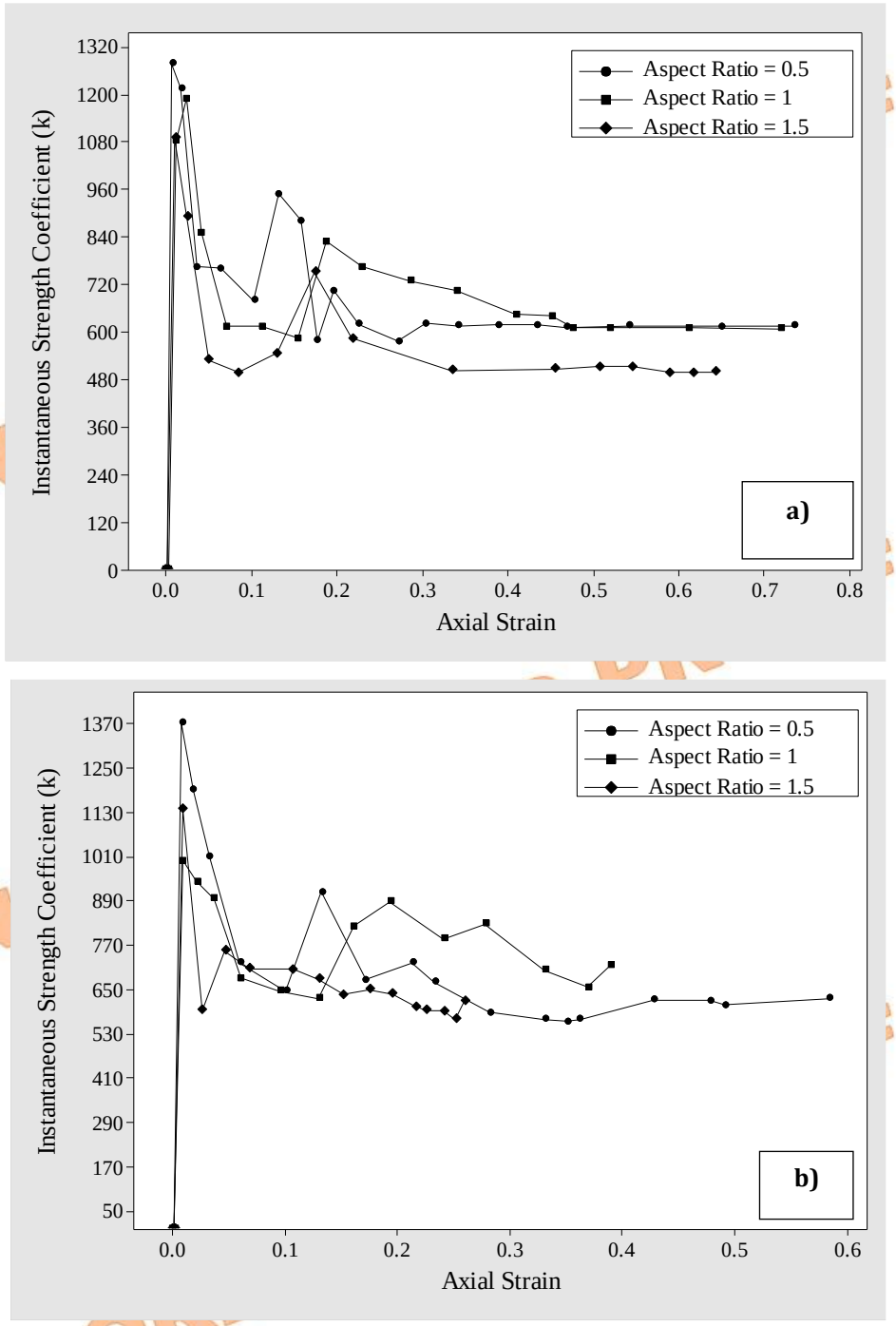

Fig. 12. Instantaneous strength coefficient of composite samples (a) as-cast (b) T6

3.2 Prediction of the Workability Parameters

The most influential parameters for predicting the workability are ε_z, σ_x, n_i, and k_i. The design of experiments for determining the relationship between the input factors, such as aspect ratio, applied load, and heat treatment, on the output responses (workability parameters) was formulated using the central composite design module of RSM. The three-level three-factor experimental design with 28 runs developed using RSM is shown in Table 1. From the quasistatic compression study, the working range of load for the composites was observed to be between 40 N and 280 N. The aspect ratio (0.5, 1, and 1.5) and applied load (40, 160, and 280) were considered as continuous factors, and the

T6 and as-cast conditions were considered as the categorical factors. The experimental design was analysed in Design Expert 11, and regression equations were generated for all the responses for each categorical factor. Based on the analysis of variance (ANOVA), the non-significant factors were identified and eliminated from the regression equations. Table 2, Table 3, Table 4, and Table 5 show the ANOVA results for ε_z, σ_x, n_i, and k_i, respectively. The significance of the developed models was evaluated using an ANOVA test for each response variable. The p-value indicates whether the model and its parameters are statistically meaningful. A model is considered significant when the p-value is below 0.05; otherwise, it is deemed non-significant. The adequacy of model fitting can be examined through lack-of-fit analysis, as well as by assessing the predicted and adjusted coefficients of determination (R^2) and the adequate precision (signal-to-noise ratio). For the model to be acceptable, the gap between the predicted R^2 and adjusted R^2 should not exceed 0.2. The regression equations developed are shown in Table 6.

Table 1. Experimental design with output responses

Run	Input Factors			Output Responses			
	Aspect Ratio	**Load (N)**	**Heat Treatment**	**Axial Strain (ε_z)**	**Axial Stress (σ_z) MPa**	**Instantaneous Strain hardening exponent (n_i)**	**Instantaneous Strength Coefficient (k_i) MPa**
1	1.5	40	as-cast	0.010724	123.7826	0.479992	1091.622
2	1.5	160	T6	0.151598	341.479	0.434794	632.194
3	1	160	T6	0.160169	367.4874	0.448219	835.1532
4	1	160	as-cast	0.191161	371.8978	0.4888	834.9802
5	1.5	280	T6	0.251886	359.1464	0.256805	568.7296
6	1	280	as-cast	0.452557	517.566	0.221558	598.5679
7	0.5	280	T6	0.224056	412.3858	0.283493	872.4595
8	1.5	160	as-cast	0.218156	357.0974	0.322596	583.576
9	1	40	T6	0.150048	301.7364	0.312808	838.5935
10	1	160	as-cast	0.187535	370.6296	0.481609	829.9081
11	1	160	as-cast	0.191161	371.8978	0.4888	834.9802
12	1	160	as-cast	0.189951	372.5343	0.48586	834.9222
13	1	160	as-cast	0.193585	371.2629	0.486016	833.7119
14	1	160	T6	0.160169	368.7395	0.445819	834.3224
15	1	160	T6	0.160169	366.8637	0.439303	820.2302
16	1	280	T6	0.009041	346.7826	0.313977	828.8347
17	0.5	160	as-cast	0.157824	402.9607	0.481136	881.6152
18	1	160	T6	0.158996	367.4874	0.445171	833.2248
19	0.5	40	as-cast	0.008032	126.2606	0.494608	1278.565
20	0.5	280	as-cast	0.34249	480.2631	0.234159	617.2275
21	0.5	160	T6	0.170322	396.4062	0.480787	1001.632
22	1.5	280	as-cast	0.616186	452.6036	0.200349	498.7112
23	1	160	T6	0.158996	365.6212	0.438409	818.7502
24	1	40	as-cast	0.012073	125.2605	0.488351	1082.853
25	1.5	40	T6	0.007044	239.5388	0.354088	822.9
26	1	160	as-cast	0.187535	370.6296	0.481609	829.9081
27	0.5	40	T6	0.171975	350.5698	0.288618	885.7612
28	1	160	T6	0.161343	370.6296	0.436376	821.5961

Table 2. ANOVA for Axial Strain (ε_z)

Source	DF	Adj SS	Adj MS	F-Value	P-Value
Model	6	0.398075	0.066346	26.58	0.000
Linear	3	0.226025	0.075342	30.19	0.000
Aspect Ratio	1	0.002727	0.002727	1.09	0.308
Load	1	0.196690	0.196690	78.81	0.000
Heat Treatment	1	0.026609	0.026609	10.66	0.004
2-Way Interaction	3	0.172049	0.057350	22.98	0.000
Aspect Ratio*Load	1	0.026885	0.026885	10.77	0.004
Aspect Ratio*Heat Treatment	1	0.020217	0.020217	8.10	0.010
Load*Heat Treatment	1	0.124948	0.124948	50.07	0.000
Error	21	0.052408	0.002496		
Lack-of-Fit	13	0.052377	0.004029	1040.38	0.000
Pure Error	8	0.000031	0.000004		
R^2	88.37%				
R^2(adjusted)	85.04%				
R^2 (predicted)	70.27%				

Table 3. ANOVA for Axial Stress (σ_z)

Source	DF	Adj SS	Adj MS	F-Value	P-Value
Model	6	228842	38140	119.09	0.000
Linear	3	149144	49715	155.22	0.000
Aspect Ratio	1	7262	7262	22.67	0.000
Load	1	141180	141180	440.81	0.000
Heat Treatment	1	702	702	2.19	0.154
Square	1	17971	17971	56.11	0.000
Load*Load	1	17971	17971	56.11	0.000
2-Way Interaction	2	61727	30864	96.37	0.000
Aspect Ratio*Heat Treatment	1	1709	1709	5.34	0.031
Load*Heat Treatment	1	60019	60019	187.40	0.000
Error	21	6726	320		
Lack-of-Fit	13	6716	517	423.29	0.000
Pure Error	8	10	1		
R^2	97.14%				
R^2(adjusted)	96.33%				
R^2 (predicted)	92.22%				

Table 4. ANOVA for Strain Hardening Exponent (n_i)

Source	DF	Adj SS	Adj MS	F-Value	P-Value
Model	5	0.233719	0.046744	37.79	0.000
Linear	3	0.079998	0.026666	21.56	0.000
Aspect Ratio	1	0.003823	0.003823	3.09	0.093
Load	1	0.068724	0.068724	55.56	0.000
Heat Treatment	1	0.007452	0.007452	6.02	0.022
Square	1	0.112226	0.112226	90.74	0.000
Load*Load	1	0.112226	0.112226	90.74	0.000
2-Way Interaction	1	0.041495	0.041495	33.55	0.000
Load*Heat Treatment	1	0.041495	0.041495	33.55	0.000
Error	22	0.027211	0.001237		
Lack-of-Fit	14	0.027049	0.001932	95.72	0.000
Pure Error	8	0.000161	0.000020		
R^2	89.57%				
R^2(adjusted)	87.20%				
R^2 (predicted)	81.71%				

Table 5. ANOVA for Instantaneous Strength Coefficient (k)

Source	DF	Adj SS	Adj MS	F-Value	P-Value
Model	4	667765	166941	48.74	0.000
Linear	3	489815	163272	47.67	0.000
Aspect Ratio	1	149528	149528	43.66	0.000
Load	1	338609	338609	98.87	0.000
Heat Treatment	1	1678	1678	0.49	0.491
2-Way Interaction	1	177950	177950	51.96	0.000
Load*Heat Treatment	1	177950	177950	51.96	0.000
Error	23	78770	3425		
Lack-of-Fit	15	78475	5232	141.90	0.000
Pure Error	8	295	37		
R^2	89.45%				
R^2(adjusted)	87.61%				
R^2 (predicted)	81.17%				

Table 6. Regression Equations

Parameter	Heat-Treatment	Regression Equation
Axial Strain (ε_z)	As-Cast	ε_z = -0.0171 - 0.0423*Aspect Ratio + 0.000951*Load + 0.000966* Aspect Ratio*Load
	T6	ε_z = 0.3216 - 0.2065*Aspect Ratio - 0.000750*Load + 0.000966 Aspect Ratio*Load
Axial Stress (σ_z)	As-Cast	σ_z = 61.2 - 25.3*Aspect Ratio + 2.631*Load - 0.0039027*Load*Load
	T6	σ_z = 307.6 - 73.1*Aspect Ratio + 1.452*Load - 0.0039027* Load*Load
Instantaneous Strain hardening exponent (n_i)	As-Cast	n_i = 0.4992 - 0.0357*Aspect Ratio + 0.001722*Load - 0.000009 Load^2
	T6	n_i = 0.2698 - 0.0357*Aspect Ratio + 0.002702*Load - 0.000009 Load^2
Instantaneous Strength Coefficient (k_i)	As-Cast	k_i = 1440.4 - 223.3*Aspect Ratio - 1.915*Load
	T6	k_i = 1100.2 - 223.3*Aspect Ratio - 0.385*Load

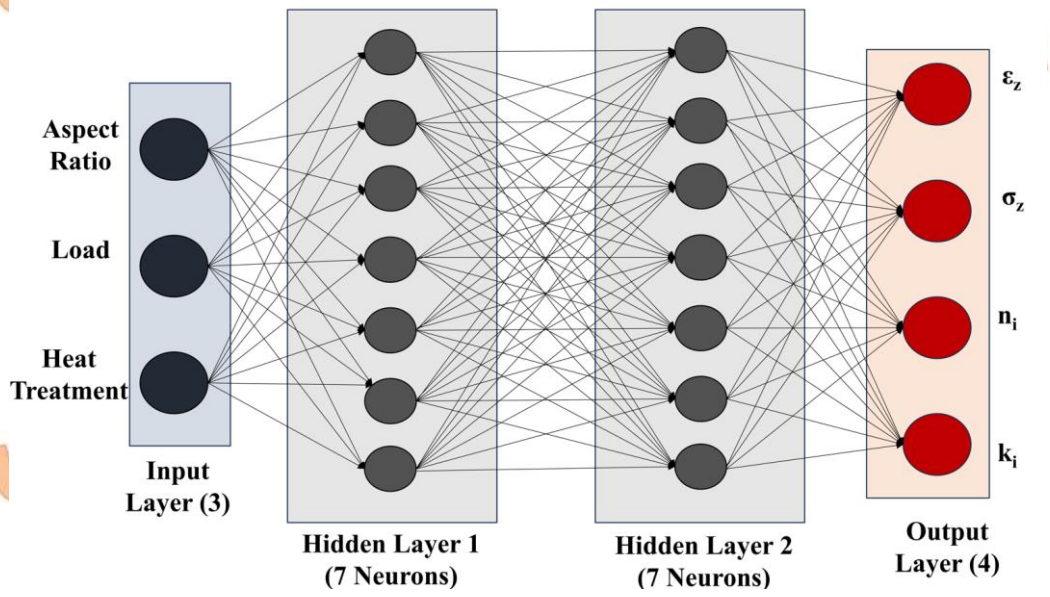

Fig. 13. ANN architecture used for predicting the workability parameters

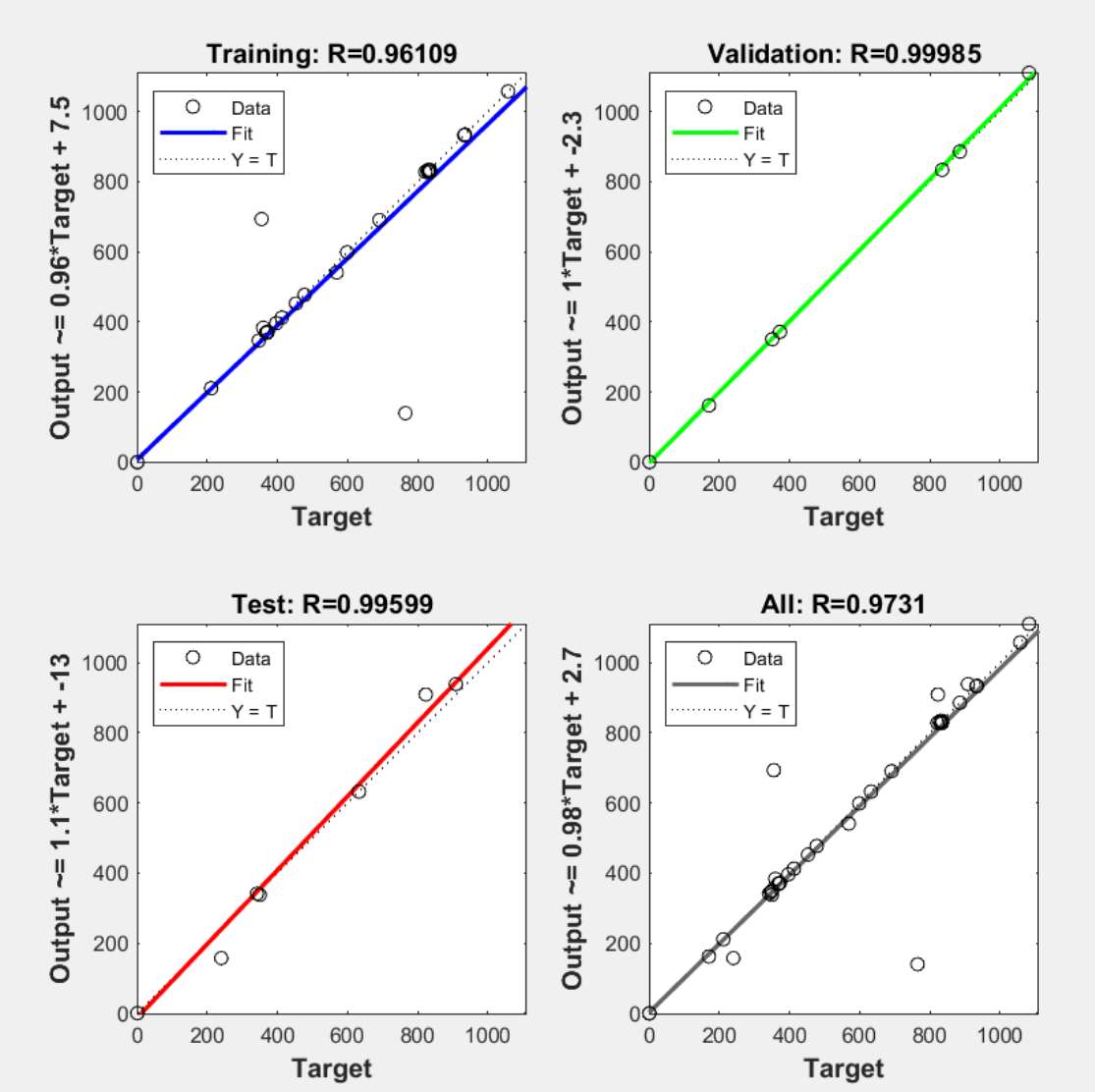

Fig. 14. Correlation plots of ANN

The artificial neural network (ANN) is one of the most powerful machine learning algorithms, which is capable of identifying the test data pattern and generating near-accurate predictions of the output parameters. The efficiency of ANN in predicting the output depends upon the number of datasets used for training, as well as the number of hidden layers and the neurons in each hidden layer. The Levenberg-Marquardt algorithm and feed-forward back propagation network type, which is capable of providing fast convergence for multi-layer neural networks, was adopted for the current work. According to the experimental design shown in Table 1, 75% of the data (21 data sets) were used for training the ANN model, and 25% of the data (7 data sets) were used for testing. The ANN model with two hidden layers having seven neurons in each layer (3-7-7-4), as shown in Fig. 13, was observed to make the most accurate prediction based on the trial-and-error tuning of the network in MATLAB. During the training stage, the network converged at 8 epochs, and the correlation plots shown in Fig. 14 were obtained. The R-values (Pearson's correlation coefficient values) for training, validating, and testing indicated that the proposed ANN model may predict accurate values of workability parameters.

The comparison between the experimental values of workability parameters and those predicted through RSM and ANN models is shown in Tables 7, 8, 9, and 10. The results show that the ANN model is capable of predicting the workability parameters in a remarkably accurate manner compared to the RSM models. The ability of ANN to capture nonlinear and intricate data patterns and execute accurate predictions may be attributed to this. The accuracy of the ANN model could be further improved by training it with a greater number of datasets.

Table 7. Predicted values of axial strain (ε_z) for the test data

S.N.	Aspect Ratio	Load (N)	Heat Treatment	Axial Strain (ε_z)		
				Experimental	RSM	ANN
1.	1.5	280	as-cast	0.61618	0.591450	0.61602
2.	1	160	T6	0.15899	0.149613	0.16007
3.	1	40	as-cast	0.01207	0.017280	0.01196
4.	1.5	40	T6	0.00704	0.039810	0.00700
5.	1	160	as-cast	0.18753	0.247320	0.19152
6.	0.5	40	T6	0.17197	0.207638	0.17173
7.	1	160	T6	0.16134	0.149613	0.16007

Table 8. Predicted values of axial stress (σ_z) for the test data

S.N.	Aspect Ratio	Load (N)	Heat Treatment	Axial Stress (σ_z)		
				Experimental	RSM	ANN
1.	1.5	280	as-cast	452.6036	453.95596	452.5132
2.	1	160	T6	365.6212	366.90960	367.6407
3.	1	40	as-cast	125.2605	134.86480	125.3903
4.	1.5	40	T6	239.5388	249.78560	236.1525
5.	1	160	as-cast	370.6296	356.50800	371.8911
6.	0.5	40	T6	350.5698	322.88560	350.3714
7.	1	160	T6	370.6296	366.90960	367.6407

Table 9. Predicted values of the instantaneous strain hardening exponent (n_i) for the test data

S.N.	Aspect Ratio	Load (N)	Heat Treatment	Instantaneous Strain Hardening Exponent (n_i)		
				Experimental	RSM	ANN
1.	1.5	280	as-cast	0.20035	0.22221	0.2003
2.	1	160	T6	0.43841	0.43602	0.4406
3.	1	40	as-cast	0.48835	0.51798	0.4885
4.	1.5	40	T6	0.35409	0.30993	0.3314
5.	1	160	as-cast	0.48161	0.50862	0.4869
6.	0.5	40	T6	0.28862	0.34563	0.2887
7.	1	160	T6	0.43638	0.43602	0.4405

Table 10. Predicted values of the instantaneous strength coefficient (k_i) for the test data

S.N.	Aspect Ratio	Load (N)	Heat Treatment	Instantaneous Strength Coefficient (k_i)		
				Experimental	RSM	ANN
1.	1.5	280	as-cast	498.7112	569.25	498.1160
2.	1	160	T6	818.7502	815.30	826.6254
3.	1	40	as-cast	1082.853	1140.5	1082.3460
4.	1.5	40	T6	822.9000	749.85	819.3970
5.	1	160	as-cast	829.9081	910.70	834.4354
6.	0.5	40	T6	885.7612	973.15	886.0961
7.	1	160	T6	821.5961	815.30	826.6254

4. Conclusion

This study investigated the workability of AA6082 composites reinforced with 7.5 wt.% MK and 1.5 wt.% nano-Si_3N_4, fabricated through ultrasonic cavitation-assisted stir casting. Cylindrical specimens with aspect ratios of 0.5, 1, and 1.5 were examined in both as-cast and T6 heat-treated conditions under quasi-static compression. The key findings are:

i. Compressive stresses increased as the aspect ratio decreased. As-cast composites with aspect ratios of 0.5 and 1 sustained compressive loading up to 50% height reduction without visible cracks. The as-cast

sample with aspect ratios 0.5 and 1 sustained maximum axial stresses and strains of 573.275 MPa,0.733 and 567.24 MPa, 0.719. The samples with an aspect ratio of 1.5 fractured prematurely at a lower load and lower axial strain (476.32 MPa and 0.664).

ii. On the other hand, all the T6-treated specimens fractured before reaching 50% reduction in height due to their increased brittleness. The T6 sample with an aspect ratio of 0.5 possessed maximum axial stress and strain of 543 MPa and 0.583.

iii. Post-compression analysis of as-cast samples revealed pore-closure as the dominant deformation mechanism, which enhanced plastic deformation. The reinforcement particles provided additional resistance to loading through dispersion strengthening. In contrast, T6-treated samples exhibited Si-rich eutectic phases that contributed to higher strength but also introduced brittleness, leading to premature fracture.

iv. The variation of the instantaneous strain hardening exponent (n_i) and strength coefficient (k_i) with axial strain (ε_z) confirmed the occurrence of both matrix work hardening in the initial deformation stage and geometric work hardening during later stages of compressive loading.

v. An experimental design with 28 runs was developed using face-centred central composite design (RSM), considering aspect ratio (0.5, 1.0, 1.5), applied load (40–280 N), and heat-treatment (as-cast and T6). Comparison of predictive models showed that the artificial neural network (ANN) consistently outperformed RSM, offering more accurate predictions of workability parameters by effectively capturing nonlinear interactions.

Nomenclature

MK	Metakaolin
RSM	Response Surface Methodology
ANN	Artificial Neural Network
SEM	Scanning Electron Microscopy
EDAX	Energy Dispersive X-ray Analysis
σ_z	True Axial Stress
σ_θ	True Hoop Stress
σ_m	Hydrostatic Stress
σ_{eff}	Effective Stress
ε_z	Axial Strain
ε_θ	Hoop Strain
n_i	Instantaneous Strain Hardening Exponent
k_i	Instantaneous Strength Coefficient
P	Load
h_0 & h_f	Heights of the cylindrical composite samples before and after deformation
α	Poisson's Ratio
D_0	Initial diameter of the cylindrical composite sample
D_{CT}	Top contact surface diameter of the cylindrical composite sample after deformation
D_{CB}	Bottom contact surface diameter of the cylindrical composite sample after deformation
DC	Average value of D_{CT} and D_{CB}
R	Pearson's Correlation Coefficient

Acknowledgements

The authors thank the management of PSG College of Technology for their support. The authors would also like to thank Dr K Logesh, Professor, Department of Mechanical Engineering, Vel Tech Rangarajan Dr Sagunthala R&D Institute of Science and Technology, Chennai and Dr. M Sumathi, Professor, Jeppiaar Institute of Technology, Chennai, for their motivation throughout the work.

Funding Statement

This research did not receive any specific grant from funding agencies in the public, commercial, or not-for-profit sectors.

Conflicts of Interest

The author declares that there is no conflict of interest regarding the publication of this article.

References

[1] Kumar, A., Singh, V.P., Singh, R.C., Chaudhary, R., Kumar, D. and Mourad, A.H.I., 2024. A review of aluminum metal matrix composites: fabrication route, reinforcements, microstructural, mechanical, and corrosion properties. Journal of Materials Science, 59(7), pp.2644-2711. https://doi.org/10.1007/s10853-024-09398-7

[2] Wu, X. and Zhang, W., 2024. A review on aluminum matrix composites' characteristics and applications for automotive sector. Heliyon, 10, e38576. https://doi.org/10.1016/j.heliyon.2024.e38576

[3] Sarmah, P. and Gupta, K., 2024. Recent advancements in fabrication of metal matrix composites: A systematic review. Materials, 17(18), p.4635.https://doi.org/10.3390/ma17184635

[4] Khalid, M.Y., Umer, R. and Khan, K.A., 2023. Review of recent trends and developments in aluminium 7075 alloy and its metal matrix composites (MMCs) for aircraft applications. Results in Engineering, 20, p.101372.https://doi.org/10.1016/j.rineng.2023.101372

[5] Bright, R.J., Selvakumar, G., Sumathi, M. and Lenin, N., 2019. Development, mechanical characterization and analysis of dry sliding wear behavior of AA6082–Metakaolin metal matrix composites. Materials Research Express, 6(12), p.126516. https://doi.org/10.1088/2053-1591/ab52aa

[6] Hillary, J.J.M., Sundaramoorthy, R., Ramamoorthi, R. and Chelladurai, S.J.S., 2022. Investigation on microstructural characterization and mechanical behaviour of aluminium 6061–CSFA/sicp hybrid metal matrix composites. Silicon, 14(17), pp.11561-11576. https://doi.org/10.1007/s12633-022-01881-7

[7] Kumar, K.R., Pridhar, T. and Balaji, V.S., 2018. Mechanical properties and characterization of zirconium oxide (ZrO2) and coconut shell ash (CSA) reinforced aluminium (Al 6082) matrix hybrid composite. Journal of Alloys and Compounds, 765, pp.171-179. https://doi.org/10.1016/j.jallcom.2018.06.177

[8] Gupta, V., Singh, B. and Mishra, R.K., 2021. Tribological characteristics of AA7075 composites reinforced with rice husk ash and carbonized eggshells. *Proceedings of the Institution of Mechanical Engineers, Part L: Journal of Materials: Design and Applications*, *235*(11), pp.2600-2613. https://doi.org/10.1177/14644207211025810

[9] Kamatchi, R.M., Muraliraja, R., Vijay, J., Bharathi, C.S., Eswar, M.K. and Padmanabhan, S., 2023. Synthesis of Newly Formulated Aluminium Composite through Powder Metallurgy using Waste Bone Material. In E3S Web of Conferences (Vol. 399, p. 03016). EDP Sciences. https://doi.org/10.1051/e3sconf/202339903016

[10] Bright, R.J. and Hariharasakthisudhan, P., 2022. Mechanical characterization and analysis of tensile fracture modes of ultrasonically stir cast Al6082 composites reinforced with Cu powder premixed Metakaolin particles. *Frattura ed Integrità Strutturale*, *16*(62), pp.426-438. https://doi.org/10.3221/IGF-ESIS.62.29

[11] Aydın, F., 2024. Recent Progress in Aluminium Matrix Composites: A Review on Tribological Performance. Transactions of the Indian Institute of Metals, 77(8), pp.1907-1922. https://doi.org/10.1007/s12666-024-03306-y

[12] Hariharasakthisudhan, P., Sudhan H.H., Karthik, S., Sathickbasha, K., Surya Rajan, B., Quasi-static compression behavior and microstructure changes in low-cost AA6061 composites. Proceedings of the Institution of Mechanical Engineers. Part C, journal of mechanical engineering science. 2022;236(9):4876-84. https://doi.org/10.1177/09544062211055339

[13] Bright, R.J., Selvakumar, G., Hariharasakthisudhan, P. and Sumathi, M., 2022. Influence of nano-Si 3 N 4 (P) hybridization on the mechanical and quasi-static compression behaviour of AA6082-Metakaolin composites. Metallic Materials/Kovové Materiály, 60(3). https://doi.org/10.31577/km.2022.3.191

[14] Dikshit, S., Gurjar, V., Dasgupta, R., Chaturvedi, S., Pathak, K.K. and Jha, A.K., 2010. Studies on cold upsetting behaviour of AA2014-based metal matrix composites, FEM simulation, and comparison with experimental results. Journal of materials science, 45, pp.4174-4179. https://doi.org/10.1007/s10853-010-4507-3

[15] Narayanasamy, R. and Pandey, K.S., 1997. Phenomenon of barrelling in aluminium solid cylinders during cold upset-forming. Journal of Materials processing technology, 70(1-3), pp.17-21. https://doi.org/10.1016/S0924-0136(97)00035-6

[16] Narayanasamy, R., Ramesh, T. and Prabhakar, M., 2009. Effect of particle size of SiC in aluminium matrix on workability and strain hardening behaviour of P/M composite. Materials Science and Engineering: A, 504(1-2), pp.13-23. https://doi.org/10.1016/j.msea.2008.11.037

[17] Narayanasamy, R., Selvakumar, N. and Pandey, K.S., 2007. Phenomenon of instantaneous strain hardening behaviour of sintered Al–Fe composite preforms during cold axial forming. Materials & design, 28(4), pp.1358-1363. https://doi.org/10.1016/j.matdes.2006.01.020

[18] Narayanasamy, R., Anandakrishnan, V. and Pandey, K.S., 2008. Effect of geometric work-hardening and matrix work-hardening on workability and densification of aluminium–3.5% alumina composite during cold upsetting. Materials & Design, 29(8), pp.1582-1599. https://doi.org/10.1016/j.matdes.2007.11.006

[19] Narayanasamy, R., Ramesh, T. and Pandey, K.S., 2006. Workability studies on cold upsetting of Al–Al2O3 composite material. Materials & design, 27(7), pp.566-

575. https://doi.org/10.1016/j.matdes.2004.12.005

[20] Sumathi, M., Selvakumar, N. and Narayanasamy, R., 2012. Workability studies on sintered Cu–10SiC preforms during cold axial upsetting. Materials & Design, 39, pp.1-8. https://doi.org/10.1016/j.matdes.2012.02.004

[21] Sivasankaran, S., Sivaprasad, K., Narayanasamy, R. and Iyer, V.K., 2010. Effect of strengthening mechanisms on cold workability and instantaneous strain hardening behavior during grain refinement of AA 6061-10 wt.% TiO2 composite prepared by mechanical alloying. Journal of Alloys and Compounds, 507(1), pp.236-244. https://doi.org/10.1016/j.jallcom.2010.07.168

[22] Jeyasimman, D. and Narayanasamy, R., 2016. Effect of coarse grain content on microstructure, cold workability and strain hardening behavior of trimodaled AA 6061 nanocomposites reinforced with multi-walled carbon nanotubes. Advanced Powder Technology, 27(4), pp.1845-1851. http://dx.doi.org/10.1016/j.apt.2016.06.018

[23] Taha, M.A., El-Mahallawy, N.A. and El-Sabbagh, A.M., 2008. Some experimental data on workability of aluminium-particulate-reinforced metal matrix composites. Journal of Materials Processing Technology, 202(1-3), pp.380-385. https://doi.org/10.1016/j.jmatprotec.2007.07.047

[24] Thangadurai, K.R. and Asha, A., 2014. Densification behavior in forming of stir casted aluminium boron carbide composite perform during cold upsetting. Applied Mechanics and Materials, 592, pp.117-121. https://doi.org/10.4028/www.scientific.net/AMM.592-594.117

[25] Sadhasivam, R.S., Ramanathan, K., Ravichandran, M. and Jayaseelan, C., 2022. Experimental investigations on microstructure, properties and workability behavior of zinc oxide reinforced Al–Si–Mg matrix composites. Silicon, *14*(5), pp.2175-2187. https://doi.org/10.1007/s12633-021-01012-8

[26] Sivasankaran, S., Narayanasamy, R., Ramesh, T. and Prabhakar, M., 2009. Analysis of workability behavior of Al–SiC P/M composites using backpropagation neural network model and statistical technique. Computational Materials Science, *47*(1), pp.46-59. https://doi.org/10.1016/j.commatsci.2009.06.013

[27] Hassani, A., Bagherpour, E. and Qods, F., 2014. Influence of pores on workability of porous Al/SiC composites fabricated through powder metallurgy+ mechanical alloying. Journal of Alloys and Compounds, 591, pp.132-142. http://dx.doi.org/10.1016/j.jallcom.2013.12.205

[28] Krishna, C.H., Dumpala, R., Davidson, M.J., Srinivasaraju, P. and Srinivasarao, G., 2020. Analysis of anisotropy in the upsetting process of AA2014 cast alloy embedded with fly ash. Proceedings of the Institution of Mechanical Engineers, Part C: Journal of Mechanical Engineering Science, 234(14), pp.2833-2841. https://doi.org/10.1177/0954406220911389

[29] Sivaraj, M. and Selvakumar, N., 2017. Effect of particle size on the deformation behaviour of sintered Al–TiC nano composites. Transactions of the Indian Institute of Metals, 70, pp.2093-2102. https://doi.org/10.1007/s12666-016-1030-5

[30] Raj, A.M., Selvakumar, N., Narayanasamy, R. and Kailasanathan, C., 2013. Experimental investigation on workability and strain hardening behaviour of Fe–C–Mn sintered composites with different percentage of carbon and manganese content. Materials & Design, 49, pp.791-801. http://dx.doi.org/10.1016/j.matdes.2013.02.002

[31] Chen, Y., Wang, L., Feng, Z. and Zhang, W., 2021. Effects of heat treatment on microstructure and mechanical properties of SLMed Sc-modified AlSi10Mg alloy. Progress in Natural Science: Materials International, 31(5), pp.714-721. https://doi.org/10.1016/j.pnsc.2021.08.003